Geophysical Research Letters

RESEARCH LETTER
10.1029/2020GL090747

Key Points:

- First observation of large-scale dayside saucers from a sounding rocket
- The saucers are estimated to originate at ~4,000 km on cusp field lines to within estimated uncertainties
- Dispersed electrons observed in the cusp were accelerated at altitudes at or above the saucer signal source region

Supporting Information:

- Supporting information

Correspondence to:

C. Moser,
Chrystal.Moser.GR@dartmouth.edu

Citation:

Moser, C., LaBelle, J., Hatch, S., Moen, J. I., Spicher, A., Takahashi, T., et al. (2021). The cusp as a VLF saucer source: First rocket observations of long-duration VLF saucers on the dayside. *Geophysical Research Letters*, *48*, e2020GL090747. https://doi.org/10.1029/2020GL090747

Received 14 SEP 2020
Accepted 1 DEC 2020

The Cusp as a VLF Saucer Source: First Rocket Observations of Long-Duration VLF Saucers on the Dayside

C. Moser[1], J. LaBelle[1], S. Hatch[2], J. I. Moen[3,4], A. Spicher[3], T. Takahashi[3], C. A. Kletzing[5], S. Bounds[5], K. Oksavik[2,4], F. Sigernes[4], and T. K. Yeoman[6]

[1]Department of Physics and Astronomy, Dartmouth College, Hanover, NH, USA, [2]Department of Physics and Technology, Birkeland Centre for Space Science, University of Bergen, Bergen, Norway, [3]Department of Physics, University of Oslo, Oslo, Norway, [4]Department of Arctic Geophysics, University Centre in Svalbard, Longyearbyen, Norway, [5]Department of Physics and Astronomy, University of Iowa, Iowa City, IA, USA, [6]Physics and Astronomy, University of Leicester, Leicester, UK

Abstract Auroral whistler-mode radio emissions called saucers are of fundamental interest because they require an unusually stationary emission process in the dynamic auroral environment, and it is a mystery how that can happen in this or similar conditions elsewhere in geospace. The Cusp Alfvén and Plasma Electrodynamics Rocket (CAPER-2), launched into the cusp, obtained the first rocket measurements of a large-scale, multiple-armed dayside saucer, similar to those observed by the DEMETER satellite, with the addition of particle measurements and ground-based measurements. Analysis of saucer shapes, directional measurements using waveforms, and ground-based data show that, accounting for estimated uncertainties, these originate at altitudes ~4,000 km within the cusp, the eastern side of which is penetrated by the rocket ~100 s after the saucers are encountered. On-board particle instruments show dispersed electron bursts in the cusp, Alfvénically accelerated at altitudes at or above the saucer sources.

Plain Language Summary Electrons, precipitating down Earth's high-latitude magnetic field lines, emit radio waves at angles to the background magnetic field, depending on frequency. When spacecrafts traverse through a region close to the source, they observe descending and ascending frequency signatures referred to as saucers. This research focused on rocket measurements of large-scale, multiarmed saucers on the dayside. Using ray-tracing software and hodogram analysis of the electric field waveforms combined with ground-based measurements, we were able to determine the source location of the saucers to be in the magnetic field's cusp at altitudes near 4,000 km. Additionally, particle measurements on-board the rocket showed time dispersed bursts of electrons typically associated with Alfvénic acceleration, which can be traced back to a source height that is equal to or above the source heights of the observed saucers. This is the first time that dayside large-scale saucers have been associated with the cusp.

1. Introduction

Very low frequency (VLF) auroral hiss is one of the most prevalent auroral radio emissions, detected by suitably instrumented spacecraft on almost every pass through aurora (reviews by LaBelle & Treumann, 2002; Sazhin et al., 1993). Satellites often observe structured hiss such as saucers, which appear as multiple nested V-shaped patterns in frequency–time spectrograms. Saucers are one of the earliest VLF phenomena reported from spacecraft, due to their distinctive appearance on spectrograms (Gurnett, 1966; Mosier & Gurnett, 1969; Smith, 1969). Saucers are of broad interest because they demonstrate a wave phenomenon that is unusually stationary despite the dynamic environment of the aurora. Original observations of saucers occurred in nightside auroral traversals, where downward going "funnel shaped" emissions were observed punctuated by upward-propagating saucers lasting tens of seconds (e.g., Gurnett & Frank, 1972, Plates 4–5). Saucers arise from propagation effects, whereby whistler-mode signals of different frequencies generated on the "resonance cone" propagate at different angles relative to the magnetic field: a satellite or rocket flying over or under the source sees a V-pattern of frequencies versus time. H. James (1976) showed how,

assuming a point source, the saucer shapes and frequencies allow the distance from satellite to source to be inferred. Temerin (1979) generalized this analysis to include line sources. Lönnquist et al. (1993) showed saucers occurring up to 13,000 km. Horita and James (1982) showed that saucers can come from sources above the satellite as well as below and argued that downward suprathermal electrons were the source. Ergun et al. (2001) showed dramatic multiple-armed saucers detected by the FAST satellite, with bursty electric fields at the vortices indicative of upward-propagating phase space electron holes, implicating these features in the chain of causation. Kasahara et al. (1995) measure wave-normal angles with the Akebono satellite confirming generation on a resonance cone.

While most observations above concentrated on nightside aurora, it was known from an early date that saucers also occur on the dayside. For example, Yoshino et al. (1981) observed saucers on the dayside as well as nightside. Pfaff et al. (1998) noted V-shape signatures with the FAST satellite as it traversed the cusp region. H. G. James et al. (2012) made significant advances based on dramatic multiple-armed saucers observed on the dayside with the DEMETER satellite. These dayside saucers lasted considerably longer than typical previously observed nightside examples, with durations up to 100 s, corresponding to up to 1,000 km given spacecraft horizontal velocities (top left example in Figure 1 of H. G. James et al., 2012). The source locations of these saucers were correspondingly inferred to be at great distances above the satellite, of order 3,000 km. Several examples were observed suggesting that large-scale saucers with high-altitude sources may be a regular feature of the dayside.

The recent Cusp Alfvén and Plasma Electrodynamics Rocket (CAPER-2) mission encountered a large-scale saucer event similar to those reported by H. G. James et al. (2012), for the first time from a sounding rocket. Rocket observations including electron spectra and electric field waveforms, combined with ground-based imager data, show a connection between this event and the cusp.

2. Data Presentation

The CAPER-2 sounding rocket launched from Andøya, Norway, at 09:27 UT on 4 January 2019, reaching an apogee of 774 km. The interplanetary magnetic field (IMF) was relatively stable, with IMF $B_z \approx -5$ nT and IMF $B_y \approx 2$–6 nT, for 1–2 h prior to launch. Under these conditions, radar backscatter typical of cusp appeared over Svalbard measured with the Super Dual Auroral Radar Network (SuperDARN) (Chisham et al., 2007) at Hankasalmi. Cusp signatures such as enhanced ionospheric density and temperature were measured by the European Incoherent Scatter Scientific Association (EISCAT) Svalbard radar using the upward-directed 42 m antenna, and red-line-dominated cusp aurora was observed over Svalbard with ground-based imagers.

The CAPER-2 payload included field and electron instruments. The electric field up to 40 kHz perpendicular to the rocket spin axis, with a spin rate of ~0.75 Hz and maintained within 10° of the background magnetic field direction, was measured with two radial double-probe antennas using 6-cm diameter probes with 3 m separation. High frequency (HF) electric fields up to 5.0 MHz were measured with a parallel axial double-probe antenna. CAPER-2 included two types of electron detectors: bagel-style detectors measured downgoing electrons in eight selected energy ranges between 220 and 625 eV and top-hat style detectors measured 0.2–12.3 keV electron distribution functions. CAPER-2 also included a flux-gate magnetometer, four needle Langmuir probes and a wave-particle correlator.

Figure 1a is a 0–2.5 MHz electric field spectrogram. For most of the flight after 200 s, the electron gyrofrequency (f_{ce}) exceeds the plasma frequency (f_{pe}); the latter appears as an upper cutoff of whistler-mode noise, descending from 1,200 kHz at 210 s (408 km) to 300 kHz at 529 s (774 km). CAPER-2 enters the cusp at 490 s (769 km), marked by the onset of low-energy downgoing electrons in Figure 1c. These electrons persist until approximately 700 s (670 km) on the downleg. During the 210 s interval in which CAPER-2 is within the cusp, intense Langmuir waves near f_{pe} appear in the HF spectrogram, and before and after this time intense whistler-mode waves occur below f_{pe}. The plasma frequency increases above its ambient level during the cusp traversal, as expected from a combination of electron impact ionization and Joule heating enhancing the scale height. Figure 1b is a 0–25 kHz VLF electric field spectrogram, showing a band of whistler-mode waves through much of the flight with lower cutoff near the lower-hybrid frequency ($f_{LH} \sim 5$ kHz). Broadband VLF waves occur below f_{LH} during the cusp traversal. Structured whistler-mode emissions at 5–20 kHz

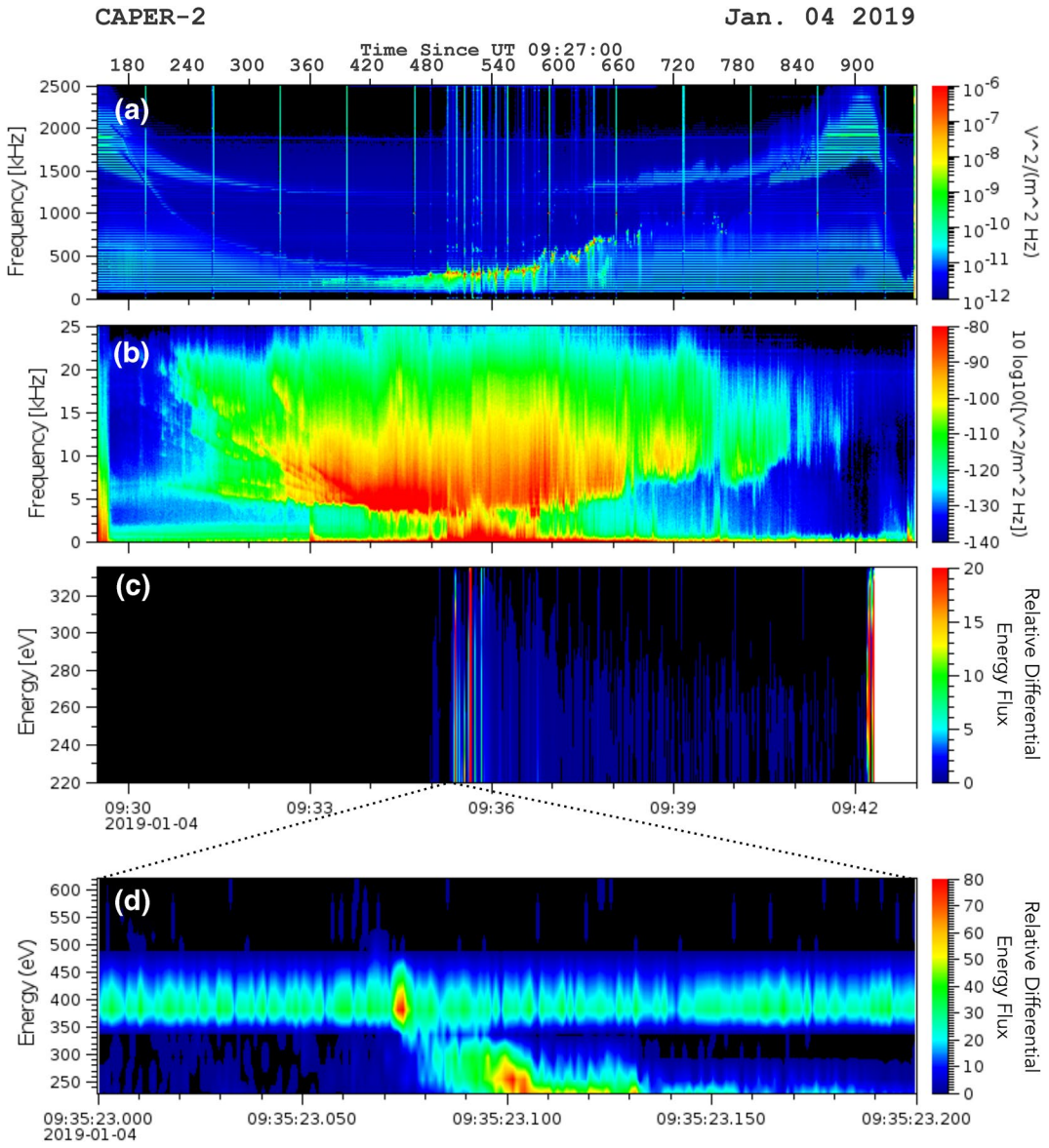

Figure 1. Survey of CAPER-2 data: (a) HF measurements. Intense plasma waves occur during the cusp crossing (~500–700 s). (b) VLF measurements. Saucer-like features above the lower-hybrid cutoff occur during 200–450 s. (c) Low-energy parallel electron measurements. An increase in counts indicates soft particle precipitation associated with the cusp. (d) Zoomed view of observed electron time–energy dispersion associated with Alfvénically accelerated electrons. HE, high frequency. VLF, very low frequency.

appear at 200 s (385 km), several hundred seconds before the cusp encounter. Whistler-mode waves in this frequency range continue during the cusp traversal but are less structured.

Figure 2 shows expanded views of the VLF spectrogram, covering 0–25 kHz and 180–450 s. Most striking are bursts of VLF waves marked by sharp lower cutoffs that descend in frequency with time. The bottom panel highlights 12 selected wave cutoffs seen in the top panel. These features resemble VLF saucers, nested cone-like features at VLF frequencies, commonly observed with spacecraft traversing the auroral region and attributed to dispersion effects (e.g., Ergun et al., 2001; H. James, 1976). However, whereas saucers typically last a few seconds in the spacecraft frame, corresponding to tens of kilometers, the wave structures encountered by CAPER-2 persist for hundreds of kilometers, similar to dayside saucers observed with the DEMETER spacecraft (H. G. James et al., 2012). The saucers observed by CAPER-2 are observed only on the equatorward side of the cusp.

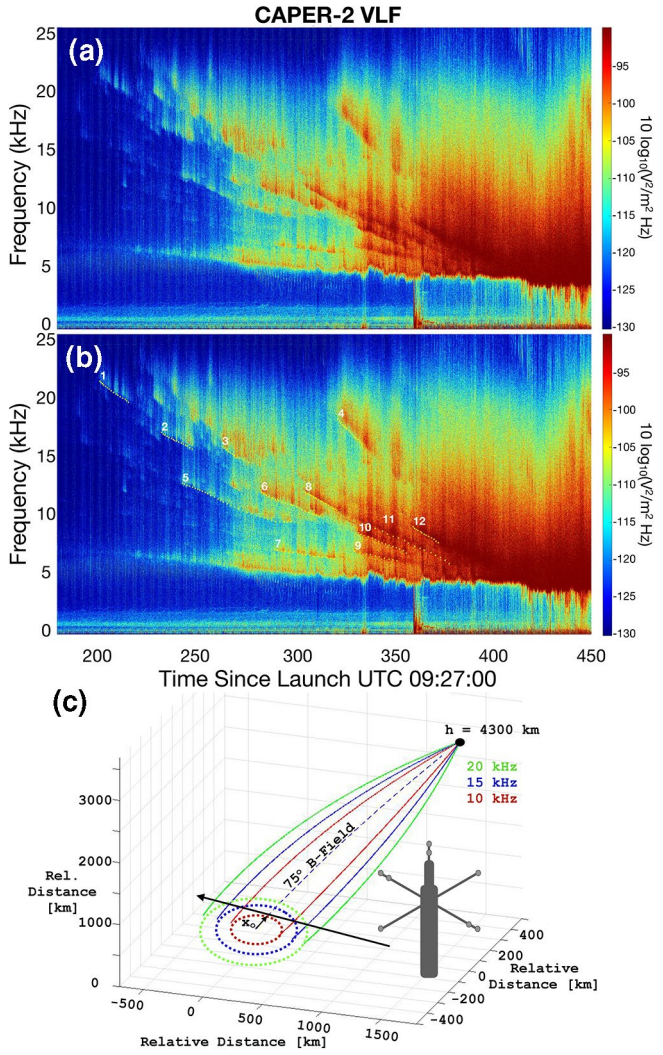

Figure 2. (a) Expanded view of saucer-like features seen in Figure 1. (b) Highlights cutoffs of 12 selected saucers. (c) Geometry for generation of saucer feature with ray paths corrected for refraction, calculated with ray-tracing code (see text).

Figure 2c illustrates the mechanism responsible for VLF saucers. The whistler mode is characterized by a resonance cone, a surface in k-space for which the index of refraction becomes large. On this resonance cone, the wave-normal direction is perpendicular to the group velocity direction. Hence, for waves on the resonance cone at the low-frequency end of the whistler range, near f_{LH}, the wave-normal direction is nearly perpendicular to the background B-field, and the ray direction is nearly parallel. For waves at the top end of the whistler range and near the lesser of f_{pe} or f_{ce}, the wave normal is nearly parallel and the ray direction nearly perpendicular. Since the auroral electrons are relatively slow (energies ≤10 keV), they interact with whistler waves of high index of refraction on the resonance cone. A spacecraft passing under this source observes descending whistler-mode frequencies until it reaches its closest approach to the source, after which it observes ascending frequencies.

In the CAPER-2 case, unlike many previous VLF saucer observations, straight-line propagation may not be valid. Therefore, a 2D ray-tracing program was employed, based on work by Kimura (1966) and updated by Burtis (1974), that traces radio wave of specified frequency and angle with respect to the background dipole magnetic field in a predefined density profile. For the electron density profile, the Kletzing et al. (1998) model was used, with the ionospheric term adjusted to match the density directly measured by CAPER-2 in the topside:

$$n(h) = n_0 e^{-(h-h_0)/r} + n_1 h^{-1.55} \quad (1)$$

where h is altitude in kilometers, n_0 = 9,636 cm^{-3}, h_0 = 496.8 km, r = 123 km, and $n_1 = 2.68 \times 10^7$ cm^{-3} corresponding to the noon sector in the Kletzing–Mozer model.

Ray tracing was done for putative sources ranging from 1,500 to 4,900 km along the 75° field line, corresponding to the invariant magnetic latitude at which CAPER-2 encountered saucers; Figure 2c shows example ray paths. A database was created of ray displacements at 500 km altitude, the average altitude of CAPER-2, both poleward and equatorward of the magnetic field line. In order to approximate the destinations of rays in 3D, interpolation between the poleward and equatorward rays was employed for rays out of the magnetic meridian plane, creating ellipses centered on the field line for each frequency and source altitude, as seen in Figure 2c. The separation distances for each frequency in a saucer event, determined from the time scale of the event and the horizontal velocity of the rocket, were fitted to all possible source height and horizontal displacements; the best fit results are listed in the auxiliary material. In this analysis, events labeled 1–4 and 12 in Figure 2b were not used because the fitting process was ineffective due to their high frequencies and short durations. The average and range of the resulting source heights are 4,300 km and 4,000–4,800 km. The average and range of the horizontal separation distance are 110 km and 70–150 km. The average and range of the time of closest approach to the source are 380 s and 330–420 s after launch. The same procedure was applied using a modified density profile with $n_1 = 9 \times 10^6$ cm^{-3} corresponding to the lower part rather than center of the distribution of measured densities on which Kletzing et al. (1998) based their model. The results, also in the auxiliary materials, show a 10%–15% lower source height but significantly later time of closest approach (because lower density implies more oblique initial ray directions for each frequency).

Whistler-mode waves in the ionosphere at frequencies well below f_{pe} or f_{ce} are approximately right-circularly polarized; i.e., the electric field of the wave rotates about the direction of propagation tracing a circle on a hodogram plot of E_x versus E_y in the plane perpendicular to the direction of propagation. CAPER-2 measures the VLF electric field vector in the plane perpendicular to the rocket spin axis which is aligned

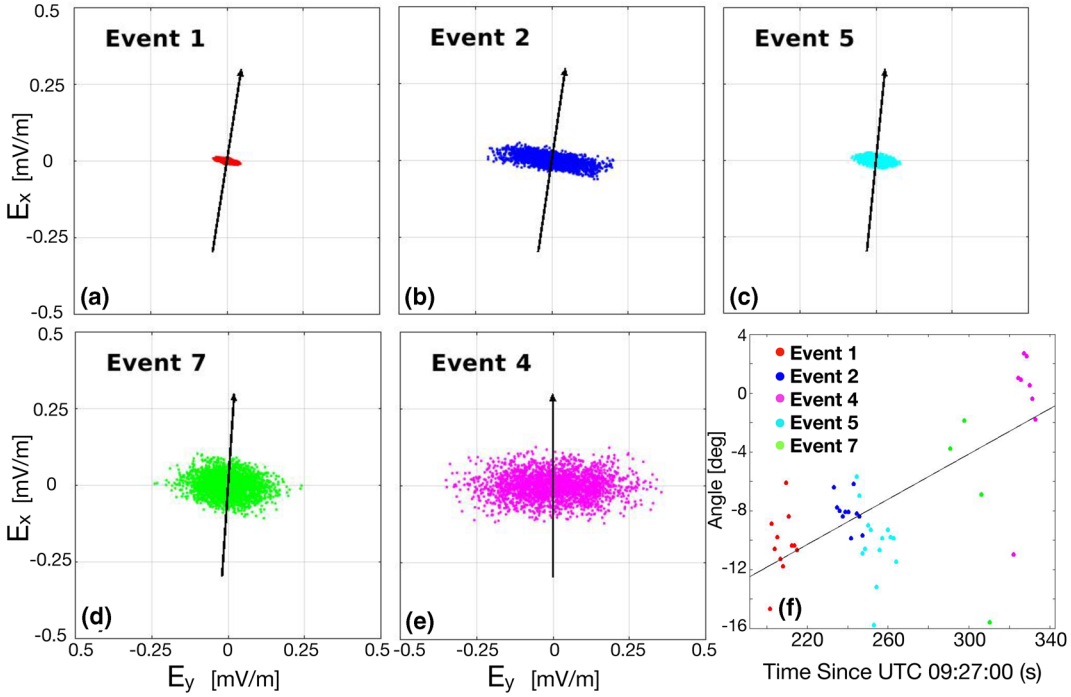

Figure 3. (a–e) Hodogram scatterplots of E_x versus E_y for five saucer signatures labeled in Figure 2. The pancake-like feature indicates that the wave arrives at an angle from source to the rocket, rather than directly downward. (f) Azimuthal angle of arrival versus flight time.

to within 10° of the magnetic field. If the circularly polarized wave propagates perpendicular to this plane, the instrument would detect the full magnitude of the electric field, yielding a circular pattern when E_x is plotted against E_y. However, if the wave propagates at an angle to the *xy*-plane the antennas detect an elliptical (pancake-shaped) pattern when E_x is plotted against E_y, which provides direction information about the incoming wave to within a 180° ambiguity.

Figures 3a–3e show E_x versus E_y hodogram scatterplots during five selected saucer-like signals, for short intervals when the electric field antennas were oriented geographically north-south and east-west, based on spacecraft attitude determined from on-board gyroscope data. The electric field components in these hodograms have been digitally filtered using a bandpass filter with bandwidth 3 kHz and center frequency corresponding to the appropriate saucer-like feature. These hodograms demonstrate the expected pancake pattern, and as expected, the pancake features remain fixed in absolute space as the rocket rotates (not shown). Furthermore, these hodograms show that the last measurements (e.g., from the saucer feature labeled 4) show east-west propagation, whereas the earliest measurements (e.g., from the feature labeled 2) are consistent with propagation coming from an angle forward (northward) of the east-west line. These measurements strongly suggest that the direction of arrival initially comes from the northwest and gradually rotates to coming from due west as the rocket flies to the east of the cusp which it penetrates about 100 s later. Figure 3f shows the inferred direction of arrival relative to the east-west line, as a function of time for short intervals within the five saucer-like features. These saucer-like features are the only ones sufficiently separated from other signals and having sufficient signal-to-noise ratio to apply the digital filter and perform the analysis described above.

3. Discussion

Figure 4a shows the CAPER-2 trajectory superposed on All-Sky Imager (ASI) images recorded at Longyearbyen, on Svalbard, in red line (6,300 Å, left panel), green line (5,577 Å, middle panel), and the ratio of red to green (right panel). Broadly over large scale, red dominates over green as expected for cusp. However, as also expected for cusp, arcs and filaments occur within the cusp which temporarily have stronger intensity

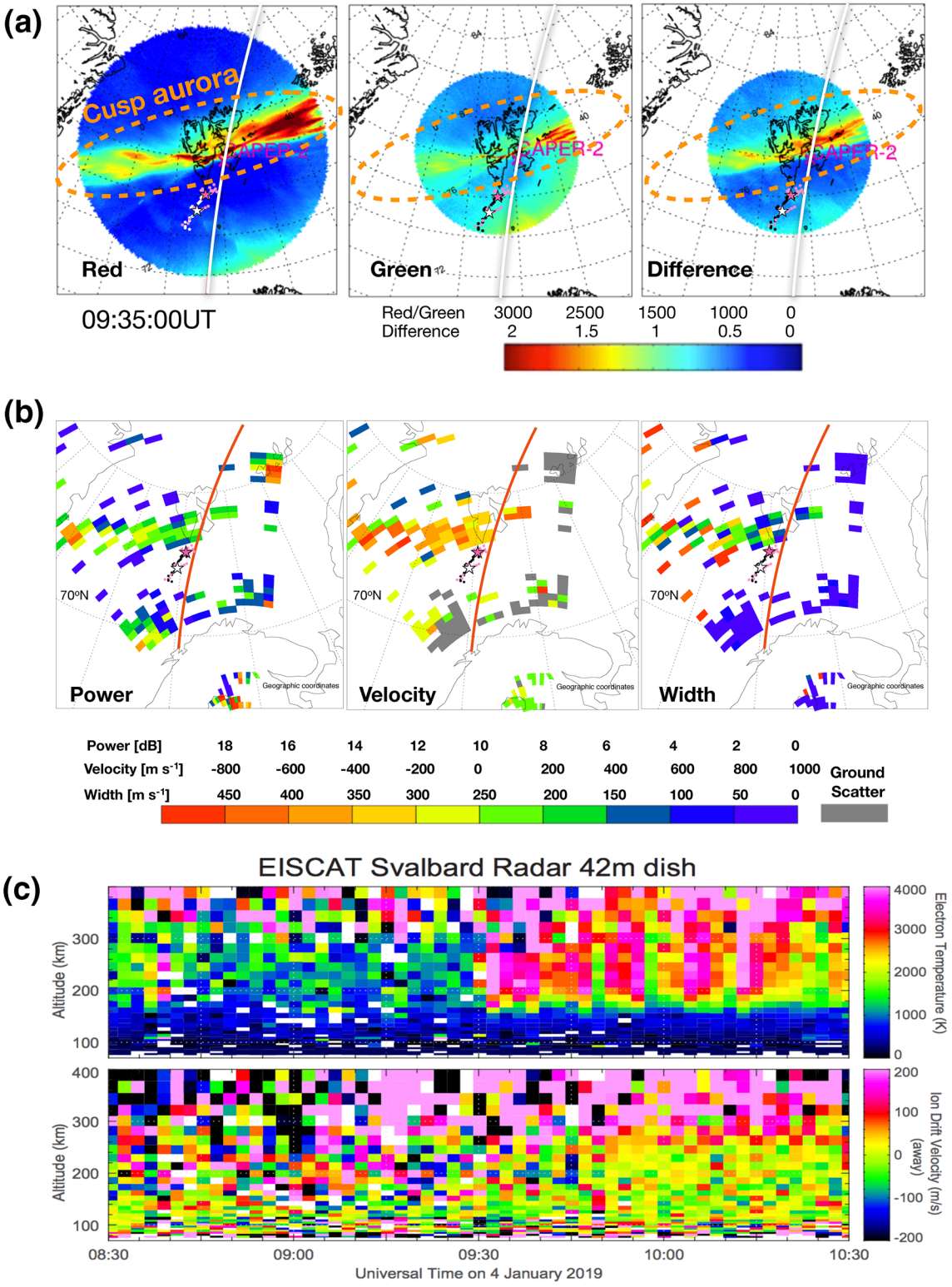

Figure 4. (a) Red (left) and green (middle), and ratio of red to green (right), line emissions observed by Longyearbyen ASI with CAPER-2 trajectory superposed. The intense red line over Svalbard is an indication of cusp aurora. (b) SuperDARN backscatter maps of Doppler power, velocity, and width. (c) Data from the EISCAT Svalbard Radar, showing onset of high electron temperature and ion upflow after 09:30 UT. In (a) and (b), stars (circle symbols) indicate average values (estimated uncertainties) of saucer sources for two example density profiles. ASI, All-Sky Imager; SuperDARN, Super Dual Auroral Radar Network; EISCAT, European Incoherent Scatter Scientific Association.

in green, for example in connection with flashing signatures of Poleward Moving Auroral Forms related to flux transfer events (Oksavik et al., 2005). These features, in evidence from sequences of images similar to Figures 4a and 4b during the CAPER-2 time interval, are a key indicator of cusp aurora (P. Sandholt et al., 2004; P. E. Sandholt et al., 1998).

Figure 4b shows maps of power, Doppler velocity, and spectral width of radar backscatter originating from decameter-scale irregularities in the cusp, measured with the Hankasalmi SuperDARN radar. Gray pixels indicate locations with ground backscatter. These data have employed the range-finding algorithm with corrections for one and a half hop ionospheric backscatter as discussed by Yeoman et al. (2008) and employed in radar studies of the cusp by Yeoman et al. (2012). Radar echoes just to the west of the CAPER-2 trajectory, where the rocket direction of arrival data indicates the source of the saucers, had wide spectral widths, strong powers, and rapid poleward velocities typical of cusp echoes (Chisham & Freeman, 2003; Yeoman et al., 2012). These observations are similar to those of Moen et al. (2001). Figure 4c shows profiles of electron temperature and ion upflow measured with the EISCAT radar located just to the west of the CAPER-2 trajectory, showing onset of high electron temperature after 09:30 UT above ~180 km, consistent with the observation of red dominated aurora in the ASI (Doe et al., 2001; Vontrat-Reberac et al., 2001), and suggesting intense precipitation and heating of electrons when CAPER-2 entered the cusp. At the same time, ion upflows occur above 250 km. Taken together, EISCAT, SuperDARN, and ASI data leave no doubt that the cusp and associated aurora extend over an extended region penetrated by CAPER-2. Dashed lines in Figure 4a indicate the approximate extent of the cusp aurora, which typically can extend more than 3–4 h in magnetic local time (Maynard et al., 1997).

As shown above, CAPER-2 provides two forms of evidence pertinent to the location of the sources of the large-scale saucer features. Fitting of suitable features to ray-traces suggests that the field line connected to the sources lies approximately 110 km off of the CAPER-2 trajectory. Hodograms of the saucer electric fields also suggest a source off of the trajectory, and because the direction of arrival shifts from being forward and to the side of the trajectory to being perpendicular to the trajectory, these data indicate that the sources are west of the trajectory. This interpretation is also favored because optical data show no aurora on the eastern side of the trajectory, which is therefore unlikely to be the source of the saucers. The star symbols in Figure 4a–4b show the average location of saucer source field line determined for two density profiles, having higher (black or white star) and lower (red star) densities in the source. The unmeasured density profile at high altitudes is clearly a source of systematic error in estimating the source location; lower densities and unknown aspects such as horizontal density gradients can significantly shift the estimated location. To some degree, random uncertainty in the estimated location is suggested by the spread of x_0 and t_0 values arising from fits to the various saucer elements. To better assess the random uncertainty, traces of the saucer features shown in Figure 2b were repeated multiple times with slight variations reflecting uncertainty in the frequency cutoffs. Circle symbols in Figures 4a and 4b show footprints of source locations determine for this ensemble of traces of saucer features, for the two different density profiles. These extend considerably toward the region of precipitation and radar backscatter and suggest that the combination of systematic and random uncertainty can explain the gap between the estimated source location and the cusp identified through ASI and radar data.

CAPER-2 included high time-resolution electron data. The electrons are measured on the rocket payload and therefore do not pertain to the same field lines as the saucer sources, but they come from within the same cusp and therefore reflect the general cusp conditions. These data show that the cusp is characterized by broadband electrons (Figures 1c and 1d), including dispersed electron bursts characteristic of Alfvénic acceleration (e.g., Kletzing & Torbert, 1994), and previously observed in the cusp (Tanaka et al., 2005); in fact, satellite data show that they are nearly a constant feature in the cusp (Chaston et al., 2007). Figure 1d shows an expanded view of a dispersed feature, having maximum energy of 550 eV and dispersion of about 20 ms. The other observed dispersed electrons had similar characteristics.

The resonant Alfvénic acceleration of these dispersed electrons occurs in an extended region corresponding roughly to where the Alfvén speed matches the speed of the electrons, above the peak in the Alfvén speed profile which is typically at 3,000–4,000 km altitude (Figure 5 of L.-J. Chen et al., 2005). Hence, it is possible that the saucer sources lie within the extended acceleration region. However, due to the low energy of the dispersed electrons, which extend only up to 600 eV or so, their velocity most likely matches the Alfvén

speed at altitudes above 10,000 km, implying that the saucer sources lie below the Alfvénic acceleration region for the dispersed electrons seen by the rocket. In either case, the observations do not rule out a connection between the Alfvénically accelerated electrons and the large-scale saucer features.

CAPER-2 encounters saucers on the equatorward side of the cusp but not on the poleward side, whereas examples shown by H. G. James et al. (2012) occur on both sides (their Figure 1), although asymmetric saucers have been observed on the nightside (H. James, 1976). Location may be important: CAPER-2 exits the cusp far to the east, whereas the inferred saucer sources may be closer to the central part of the cusp. CAPER-2 is also at a lower altitude on the poleward side of the cusp than the equatorward side, although the difference is only 100 km.

Similar to those observed by H. G. James et al. (2012), the CAPER-2 saucers are intermittent or "truncated." Durations of the pieces of saucers ranged from 5 to 50 s. As noted by H. G. James et al. (2012), this presents a challenge for theory because the sources must be stationary for these time intervals.

In summary, the CAPER-2 rocket detected large-scale dayside VLF saucers for the first time from a sounding rocket. Ray tracing and hodogram analysis of the electric field data, combined with ground-based data, show that to within estimated uncertainties, the saucers originate from ~4,000 km altitude in the cusp aurora east of the trajectory identified in optical and radar images. These measurements leave little doubt that the origin of the observed saucers is in the cusp, which is in fact the only significant region of electron precipitation in the vicinity of the trajectory. The rocket data show no electron precipitation for >500 km south of the cusp encounter. These measurements highlight the advantage of a coordinated campaign of rocket and ground-based measurements that provides both local and global context via both in situ and remote observations. Furthermore, the rocket-based particle data suggest that Alfvénic electron acceleration occurs above or in the same altitude range as the saucer sources.

Data Availability Statement

Data from the CAPER-2 mission referenced within this article can be found at: https://phi.physics.uiowa.edu/science/tau/data0/rocket/SCIENCE/CAPERII_Mission/

Acknowledgments
Authors thank David McGaw, Jeff Dolan, and Espen Trondsen for instrument engineering support; NASA, NSROC, and ASC personnel for supporting launch and payload functions; and KHO, UiO, and UNIS personnel for supporting ground-based data from Svalbard. The Research Council of Norway supported S. Hatch, K. Oksavik, and F. Sigernes through grant 223252 and J. I. Moen, A. Spicher, and T. Takahashi through grant 275653. Work by S. Hatch was also supported by the European Space Agency, EO Science for Society contract 4000126731. Research at Dartmouth and University of Iowa was supported by NASA grant NNX17AF92G.
EISCAT is an international association supported by research organizations in China (CRIRP), Finland (SA), Japan (NIPR and ISEE), Norway (NFR), Sweden (VR), and the United Kingdom (UKRI): https://eiscat.se/scientist/data/

References

Baker, K., Greenwald, R., Ruohoniemi, J., Dudeney, J., Pinnock, M., Newell, P., et al. (1990). Simultaneous HF-radar and DMSP observations of the cusp. *Geophysical Research Letters*, *17*(11), 1869–1872.
Burtis, W. (1974). *User's guide to the Stanford VLF raytracing program*. Stanford, CA: Radioscience Laboratory, Stanford Electronics Laboratories, Stanford University.
Chaston, C., Carlson, C., McFadden, J., Ergun, R., & Strangeway, R. (2007). How important are dispersive Alfvén waves for auroral particle acceleration? *Geophysical Research Letters*, *34*, L07101. https://doi.org/10.1029/2006GL029144
Chen, L.-J., Kletzing, C. A., Hu, S., & Bounds, S. R. (2005). Auroral electron dispersion below inverted-V energies: Resonant deceleration and acceleration by Alfvén waves. *Journal of Geophysical Research*, *110*, A10S13. https://doi.org/10.1029/2005JA011168
Chisham, G., & Freeman, M. (2003). A technique for accurately determining the cusp-region polar cap boundary using SuperDARN HF radar measurements. *Annales geophysicae*, *21*, 983–996.
Chisham, G., Lester, M., Milan, S., Freeman, M., Bristow, W., Grocott, A., et al. (2007). A decade of the Super Dual Auroral Radar Network (SuperDARN): Scientific achievements, new techniques and future directions. *Surveys in Geophysics*, *28*(1), 33–109.
Doe, R., Kelly, J., & Sánchez, E. (2001). Observations of persistent dayside f region electron temperature enhancements associated with soft magnetosheathlike precipitation. *Journal of Geophysical Research*, *106*(A3), 3615–3630.
Ergun, R., Carlson, C., McFadden, J., Strangeway, R., Goldman, M., & Newman, D. (2001). Electron phase-space holes and the VLF saucer source region. *Geophysical Research Letters*, *28*(19), 3805–3808.
Gurnett, D. A. (1966). A satellite study of VLF hiss. *Journal of Geophysical Research*, *71*(23), 5599–5615.
Gurnett, D. A., & Frank, L. A. (1972). VLF hiss and related plasma observations in the polar magnetosphere. *Journal of Geophysical Research*, *77*(1), 172–190.
Horita, R., & James, H. (1982). Source regions deduced from attenuation bands in VLF saucers. *Journal of Geophysical Research*, *87*(A11), 9147–9153.
James, H. (1976). VLF saucers. *Journal of Geophysical Research*, *81*(4), 501–514.
James, H. G., Parrot, M., & Berthelier, J.-J. (2012). Very-low-frequency saucers observed on DEMETER. *Journal of Geophysical Research*, *117*, A09309. https://doi.org/10.1029/2012JA017965
Kasahara, Y., Yoshida, K.-I., Matsuo, T., Kimura, I., & Mukai, T. (1995). Propagation characteristics of auroral hiss observed by Akebono satellite. *Journal of Geomagnetism and Geoelectricity*, *47*(6), 509–525.
Kimura, I. (1966). Effects of ions on whistler-mode ray tracing. *Radio Science*, *1*(3), 269–283.
Kletzing, C., & Hu, S. (2001). Alfvén wave generated electron time dispersion. *Geophysical Research Letters*, *28*(4), 693–696.
Kletzing, C., Mozer, F., & Torbert, R. (1998). Electron temperature and density at high latitude. *Journal of Geophysical Research*, *103*(A7), 14837–14845.

Kletzing, C., & Torbert, R. (1994). Electron time dispersion. *Journal of Geophysical Research*, *99*(A2), 2159–2172.
LaBelle, J., & Treumann, R. A. (2002). Auroral radio emissions, 1. Hisses, roars, and bursts. *Space Science Reviews*, *101*(3–4), 295–440.
Lönnqvist, H., André, M., Matson, L., Bahnsen, A., Blomberg, L., & Erlandson, R. (1993). Generation of VLF saucer emissions observed by the Viking satellite. *Journal of Geophysical Research*, *98*(A8), 13565–13574.
Maynard, N., Weber, E., Weimer, D., Moen, J., Onsager, T., Heelis, R., & Egeland, A. (1997). How wide in magnetic local time is the cusp? An event study. *Journal of Geophysical Research*, *102*(A3), 4765–4776.
Moen, J., Carlson, H., Milan, S., Shumilov, N., Lybekk, B., Sandholt, P., & Lester, M. (2001). On the collocation between dayside auroral activity and coherent hf radar backscatter. *Annales geophysicae*, *18*, 1531–1549.
Mosier, S. R., & Gurnett, D. A. (1969). VLF measurements of the Poynting flux along the geomagnetic field with the Injun 5 satellite. *Journal of Geophysical Research*, *74*(24), 5675–5687.
Oksavik, K., Moen, J., Carlson, H., Greenwald, R., Milan, S., Lester, M., et al. (2005). Multi-instrument mapping of the small-scale flow dynamics related to a cusp auroral transient. *Annales geophysicae*, *23*, 2657–2670.
Pfaff, R., Clemmons, J., Carlson, C., Ergun, R., McFadden, J., & Mozer, F., et al. (1998). Initial fast observations of acceleration processes in the cusp. *Geophysical Research Letters*, *25*(12), 2037–2040.
Rice, W. (1997). A ray tracing study of VLF phenomena. Ph.D. dissertation, University of Natal, Durban, South Africa.
Sandholt, P., Farrugia, C., & Denig, W. (2004). *Dayside aurora and the role of imf\by\/\bz\: Detailed morphology and response to magnetopause reconnection (Tech. Rep.)*. Hanscom AFB, MA: Air Force Research Lab, Space Vehicles Directorate.
Sandholt, P. E., Farrugia, C. J., Moen, J., Noraberg Ø., Lybekk, B., Sten, T., & Hansen, T. (1998). A classification of dayside auroral forms and activities as a function of interplanetary magnetic field orientation. *Journal of Geophysical Research*, *103*(A10), 23325–23345.
Sazhin, S., Bullough, K., & Hayakawa, M. (1993). Auroral hiss: A review. *Planetary and Space Science*, *41*(2), 153–166.
Sigernes, F., Dyrland, M., Brekke, P., Chernouss, S., Lorentzen, D. A., Oksavik, K., & Deehr, C. S. (2011). Two methods to forecast auroral displays. *Journal of Space Weather and Space Climate*, *1*(1), A03.
Smith, R. (1969). VLF observations of auroral beams as sources of a class of emissions. *Nature*, *224*(5217), 351–352.
Tanaka, H., Saito, Y., Asamura, K., Ishii, S., & Mukai, T. (2005). High time resolution measurement of multiple electron precipitations with energy–time dispersion in high-latitude part of the cusp region. *Journal of Geophysical Research*, *110*, A07204. https://doi.org/10.1029/2004JA010664
Temerin, M. (1979). A comment on the source region of VLF saucers. *Journal of Geophysical Research*, *84*(A11), 6691–6693.
Vontrat-Reberac, A., Fontaine, D., Blelly, P.-L., & Galand, M. (2001). Theoretical predictions of the effect of cusp and dayside precipitation on the polar ionosphere. *Journal of Geophysical Research*, *106*(A12), 28857–28865.
Yeoman, T., Chisham, G., Baddeley, L., Dhillion, R., Karhunen, T., Robinson, T., et al. (2008). Mapping ionospheric backscatter measured by the SuperDARN HF radars—Part 2: Assessing SuperDARN virtual height models. In Annales geophysicae (Vol. 26, 843–852).
Yeoman, T., Wright, D., Engebretson, M., Lessard, M., Pilipenko, V., & Kim, H. (2012). Upstream-generated Pc3 ULF wave signatures observed near the Earth's cusp. *Journal of Geophysical Research*, *117*, A03202. https://doi.org/10.1029/2011JA017327
Yoshino, T., Ozaki, T., & Fukunishi, H. (1981). Occurrence distributions of VLF hiss and saucer emissions over the southern polar region. *Journal of Geophysical Research*, *86*(A2), 846–852.